J Nanostruct 16(1): 1042-1057, Winter 2026

RESEARCH PAPER

# Cold Sintering Process Of HA-PEEK Nanocomposite for Bone Regeneration Application

*Hawraa Oday Abbas [1]*, Hanaa Areer Smeigb [1], Zuhair Jabbar Abdul Ameer [2]*

[1] *Department of Materials Engineering, University of Technology, Baghdad, Iraq*

[2] *Department of Prosthetics and Orthotics Engineering, College of Engineering, Kerbala University, Iraq*

**ARTICLE INFO**

***Article History:***
*Received 05 September 2025*
*Accepted 27 December 2025*
*Published 01 January 2026*

***Keywords:***
*Bone Regeneration*
*Cold sintering process*
*PEEK*
*Taguchi method*

**ABSTRACT**

A novel technique of very low-temperature sintering named the Cold sintering process to produce Highly dense samples of hydroxyapatite-polyetheretherketone composites. The direct mixing method is a powder-preparation method to fabricate a unique composite. This study aimed to determine the optimum cold sintering parameters in producing HA-PEEK composites using the Taguchi method. The sintering temperature, pressure, holding time, and PEEK content were selected as the production parameters. The samples are characterized using scanning electron microscope (SEM), X-ray energy dispersive spectrometry (EDS), X-ray diffractogram (XRD), and transition electron microscope (TEM). Also, physical and mechanical properties measurements were detected, include density, water contact angle, Brunauer, Emmett, and Teller (BET), hardness and indirect tensile strength (DTS). It can be observed that the optimum cold sintering parameters for high densities (99%) and hardness (502 Hv) are 300 °C, 250 bar, 30 minutes, and 10% PEEK content. Also, the tensile strength has been improved with the addition of PEEK. The results of the biological response indicate that apatite islands developed on the HA-PEEK composite after 14 days of immersion in SBF. Additionally, in vitro test, the HA-PEEK composite exhibited good pre-osteoblast cell (MC3T3-E1) adhesion, spreading, and proliferation. In summary, our study offers a strategy for creating high-performance ceramic-polymer composites using the cold sintering procedure, which makes a good candidate for application in orthopaedic and dental implants.

**How to cite this article**
*Oday Abbas H., Smeigb H.A, Abdul Ameer J. Cold Sintering Process Of HA-PEEK Nanocomposite for Bone Regeneration Application. J Nanostruct, 2026; 16(1):1042-1057. DOI: 10.22052/JNS.2026.01.093*

## INTRODUCTION

Polyetheretherketone (PEEK) is the most common type of high-temperature thermoplastic polymer used in the biomedical field, especially for an interbody fusion cage [1]. Due to the aromatic backbone molecular chains of PEEK's chemical structure, resulting a good stability in the sterilization process, chemicals, and resistance to high-temperature. Furthermore, PEEK is biocompatible, wear-resistant, and radiolucent [2]. Due to its mechanical analogies to human cortical bone, PEEK minimizes the stress-shielding effect that metal implants typically induce. PEEK does not directly connect to the bone after implantation because it is physiologically inert and prevents full integration with the surrounding bone [3].

* *Corresponding Author Email: hawraaoday1992@gmail.com*

The closest pure synthetic substitute for the human bone mineral is synthetic hydroxyapatite (HA) with the chemical formula $Ca_{10}(PO_4)_6(OH)_2$, which is bioactive and biocompatible [4]. HA possesses osteoconductive abilities and osteointegration, so it is an excellent candidate for biomedical applications as a bone substitute [5].

In recent years, there has been plenty of research interest in developing polymeric composites used in a load-bearing application (hard tissue) [1]. One of the best candidates among them is HA/PEEK because of its combination properties of good bioactivity of hydroxyapatite and excellent mechanical properties of PEEK [6].

Traditionally, different routes have been used to prepare HA-PEEK composites, with ceramic materials dispersed in the polymeric matrix, such as compounding and injection molding [7-10], Compression molding [11,12], Pressureless sintering [13-15], and Selective laser sintering (SLS) [16-18]. In all the methods mentioned, because of the differences in sintering temperatures between polymers and ceramics, resulting very difficult fabrication of ceramic matrix composites due to damaging the polymers at high temperatures. HA often sinters at temperatures above 1000°C; this range of temperatures is impossible for treating polymeric materials simultaneously. This problem can be solved by using a new low-temperature (~300 ◦C) sintering technique named Cold Sintering Process (CSP) with Ts/Tm> 0.2. This technique potentially provides a manufacturing route with fast densification and lower energy costs to increase the throughput of the process [19]. The processing parameters and sintering mechanism of cold sintering are different from those of conventional high-temperature sintering techniques. At a solid-liquid interface, CSP takes place to produce a highly dense material. Instead of proposing a solid-state diffusion at high sintering temperatures [20, 21]. In CSP, the transient phase is often used, which is liquid or a liquid mixer to facilitate mass transport. Uniaxial pressure applied to the die encourages particle rearrangement. A dissolution-precipitation mechanism occurred after the temperature was increased to about 100–300 °C in the presence of pressure and a transient liquid phase. Giving rise to densification and potential grain growth [22]. Due to lower ceramic sintering temperatures, polymers, nanoparticles, and metals may now be incorporated into ceramic matrix composites. The greatest advantage of CSP technology since it enables the design of novel composite materials with unique characteristics such as ZnO–PTFE [23], $Na_{0.5}Bi_{0.5}MoO_4$-$Li_2MoO_4$ [24], ZnO – PDMS [25], ZnO-$BaTiO_3$ [26], $Al_2O_3$-NaCl [27], and ZnO -PEEK [19].

This study showed the possibility of integrating PEEK in the HA matrix by directly mixing using the cold sintering method. Artificial intelligence (Taguchi method) is used, for the first time, to design the cold-sintering experiments to determine

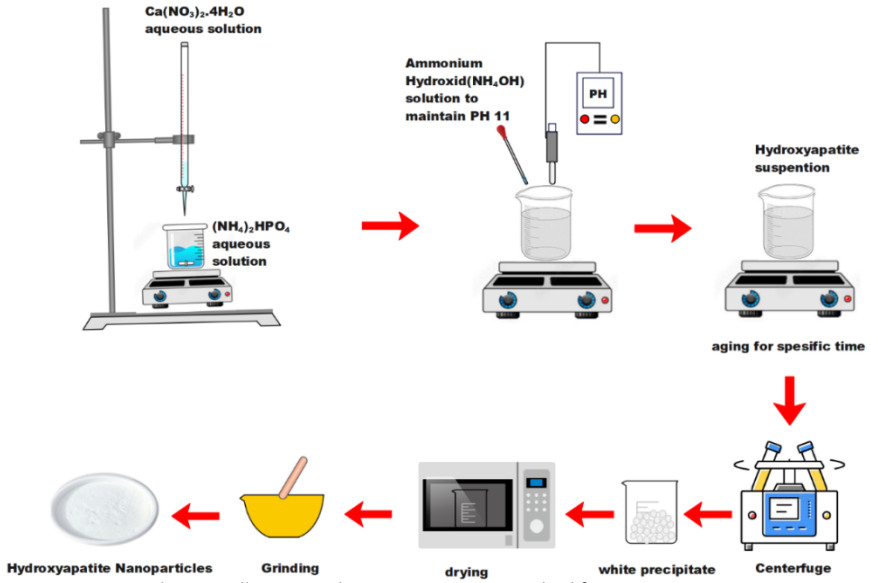


Fig. 1. Schematic illustrating the co-precipitation method for preparing Nano-HA.

the optimum production parameters, which results in maximizing density (%), hardness (Hv), and indirect tensile strength (MPa). The relative densities, microstructures, and mechanical, physical properties were studied in detail. The results indicate that the cold sintering process could produce high-performance composites with excellent biological response.

## MATERIALS AND METHODS

### *Materials*

Calcium nitrate tetrahydrate [$Ca(NO_3)_2 \cdot 4H2O$, Fluka, NLT 99%], diammonium hydrogen phosphate [$(NH_4)_2HPO_4$, Fluka, NLT 99%], ammonium hydroxide solution [$NH_4OH$, Fluka, Min. 28%], hydrochloric acid [HCl, Fluka, Min. 37%] were used as such without further purification. PEEK, with an average particle size of 8 µm (~99%), Was purchased from jilin joinature Polymer co.,ltd. ethanol [C2H6O, Qualigenes, NLT 99.5%].

### *Synthesis of Nano-HA*

Nano-HA powders used in this work were mainly synthesized via the co-precipitation method, as shown in Fig. 1. By dissolving the desired amount of diammonium hydrogen phosphate (APH, 0.100M) and calcium nitrate (CN, 0.167 M) in double distilled water at 25°C using magnetically stirring for 45 min. A digital pH meter (Systronics 335, India) was used to measure the pH of the prepared solutions. Concentrated $NH_4OH$ was used to adjust the pH of these solutions to 10.5-11 in whole experiments. With continuous stirring, 100 ml of the CN solution was slowly added dropwise to 100 ml of the APH solution. The white precipitate was subjected to aqueous washes followed by methanol washes after aging for a specific duration at 25°C. The resulting gel was oven-dried in the air at 120°C.

### *Cold sintering process*

The optimum production parameters for cold sintering HA-PEEK composites are determined using the Taguchi method. Table 1 explains the most important production parameters (Cold sintering temperature (°C), Pressure (MPa),

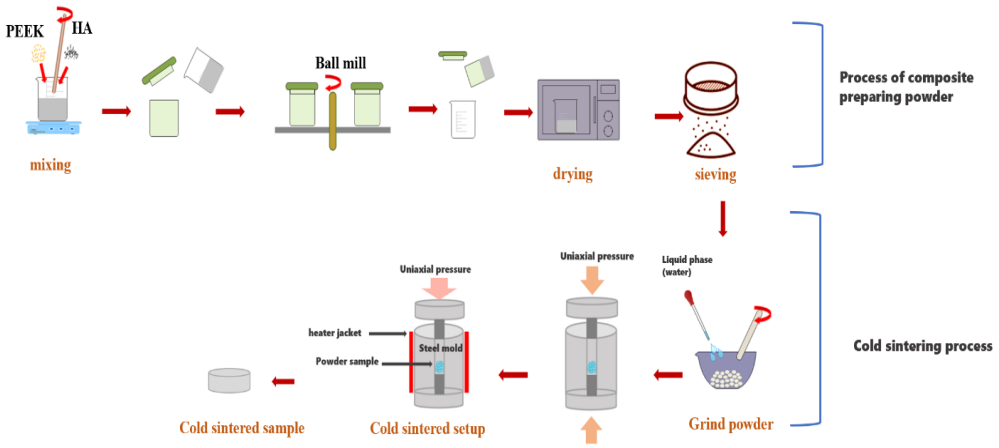


Fig. 2. Schematic illustrating the cold sintering process for the production of Nano HA-PEEK composite

Table 1. Nano HA-PEEK composite production Parameters and their levels.

| n | parameters | Levels | | | |
|---|---|---|---|---|---|
| | | 1 | 2 | 3 | 4 |
| 1 | Temperature (◦C) | 200 | 250 | 300 | 350 |
| 2 | Pressure (MPa) | 200 | 300 | 400 | 500 |
| 3 | Holding time(min) | 30 | 60 | 90 | 120 |
| 4 | PEEK content(wt%) | 10 | 20 | 30 | 40 |

Holding time(min), PEEK content (wt%)) necessary to produce Nano HA-PEEK composite and their levels; each test was repeated twice at least. 1g Nano HA-PEEK powders are wetted using 0.13 g aqueous solution (1.5 mol/L) of acetic acid and mixed using an agate mortar. According to the Taguchi Experiments Plan, as shown in Table 2, the wet powders were placed into a steel die and then cold sintered. The sample was then allowed to cool naturally to room temperature. in this study, $L_{16}(4^4)$ orthogonal factorial design was employed.

*Design of Experiment (DOE)*

The Design of Experiments (DOE) is a crucial statistical technique that employs Taguchi orthogonal arrays (OAs) to systematically investigate controllable factors and their associated responses at multiple levels. This approach reduces the number of tests required, saving both time and resources [28]. According to the Taguchi method, the L16 orthogonal array (OA) with four parameters (factors) and four levels was the most suitable for the experimental activities. Minitab 21 software was used to analyze the sintering data, and randomized OAs, starting from trial 1 and ending with trial 16, were used to perform 16 sets of the cold sintering tests. The experimental results for the cold sintering process experiments are shown in Table 2. For this study, the $L_{16}$ orthogonal array was selected, consisting of sixteen experiments. Taguchi's loss function transformed the discrepancy between experimental data and targets into an S/N ratio, signifying the mean-to-standard deviation ratio. Taguchi utilizes signal and noise to represent desired and undesired response values. The S/N ratio is classified into three categories based on the preferred response level: the lower-the-better, the medium-the-better, and the larger-the-better. In all three problems, the goal is to maximize the SN ratio. According to the Taguchi method, maximizing the SN ratios reduces the variance on the one hand and increases the signal on the other hand [29].

In this study, the larger-the-better level is used to characterize the responses. Performance statistics formulas of the "larger-the-better" characteristic to determine the optimum level of the parameters are as Eq. 1 [29].

$$SN_L = 10\log\frac{1}{n}\sum_{n=1}^{n}\frac{1}{y^2} \quad (1)$$

Table 2. $L_{16}(4^4)$ Orthogonal factorial Taguchi experimental design.

| n | Temperature | Pressure | Holding time | Water content |
|---|---|---|---|---|
| 1 | 200 | 100 | 30 | 10 |
| 2 | 200 | 150 | 60 | 20 |
| 3 | 200 | 200 | 90 | 30 |
| 4 | 200 | 250 | 120 | 40 |
| 5 | 250 | 100 | 60 | 30 |
| 6 | 250 | 150 | 30 | 40 |
| 7 | 250 | 200 | 120 | 10 |
| 8 | 250 | 250 | 90 | 20 |
| 9 | 300 | 100 | 90 | 40 |
| 10 | 300 | 150 | 120 | 30 |
| 11 | 300 | 200 | 30 | 20 |
| 12 | 300 | 250 | 60 | 10 |
| 13 | 350 | 100 | 120 | 20 |
| 14 | 350 | 150 | 90 | 10 |
| 15 | 350 | 200 | 60 | 40 |
| 16 | 350 | 250 | 30 | 30 |

In the above equations, y is the performance value (in this study hardness, relative density, or indirect strength). n is the number of repeated experimental tests.

Table 2. $L_{16}(4^4)$ Orthogonal factorial Taguchi experimental design

*Chemical and morphological characterization*

X-ray diffraction (XRD, Shimadzu, Japan) using a Cu target is used to examine the crystalline phases of nano HA powders and nano HA-PEEK composites. The diffraction angles (2Θ) were set between 10 and 60. Phases were identified by comparing the sample diffraction pattern with reference cards from the ICDD-JCPDS database.

A field emission scanning electron microscope (FE-SEM, JSM-6701F, JEOL, Tokyo, Japan) is used to characterize the surface morphology of pure nano-HA and the optimum nano-HA-PEEK composite surfaces. Before FE-SEM observation, all samples were coated with gold for 1 minute. Energy dispersive X-Ray spectroscopy (EDS) was also recorded using the same equipment to confirm the element in the prepared sample and help to calculate the Ca/p ratio after immersion the sample in SBF for 14 days.

*Mechanical properties*

The diametral tensile strength (DTS) of the sintered HA samples was found by compressing the samples (12mm diameter and 5mm thickness) using universal test instrument (Instron 5500R, USA), which was placed on its side between the two plates of Instron 5500R machine, at a crosshead speed of 0.5 mm/min until failure. The DTS (MPa) was calculated from the Eq. 2 [30]:

$$\mathrm{DTS} = \frac{2F_{max}}{\pi . t . d} \tag{2}$$

where $F_{max}$ is the failure load, d is the diameter, and t is the thickness of the sample. Vickers microhardness (HV) was also tested using Shimadzu Microhardness Tester (HMV-2L). A force (P) with a 1.961 N load and 15 s dwell time to obtain an indentation with crack propagation. Six points were chosen and measured in different positions of each sample to get an average value.

*Physical properties*

Brunauer, Emmett, and Teller (BET) method was used to measure the specific surface area and the grain size of the prepared powders. The powder was heated to 150 °C for 2 hours to eliminate any contaminants that had been released; then, the samples were made by evacuating the heated powder. After cooling with liquid nitrogen, the produced samples are examined by determining the volume of $N_2$ adsorbed at particular pressures.

A contact angle measuring device (SL200B, Kono, USA) is utilized to measure the contact angles of pure Nano HA and the optimum nano HA-PEEK composite surfaces by using the sessile drop method with a 2 mL D.I. water droplet measured at room temperature. In order to provide an average and standard deviation, six samples in each stage were used.

Archimedes' principle, as described in the ASTM B 311-08 standard, was used to calculate all sample densities using the Eq. 3:

$$\mathrm{RD} = \frac{\rho}{\rho_k} \times 100 \tag{3}$$

where RD = Relative density (%); ρ = Experimentally measured density (gr/cm$^3$); $\rho_c$= Theoretical density calculated based on powder mixture ratios (gr/cm$^3$) (Eq. 4).

$$\rho_c = \frac{1}{\left[\frac{M}{\rho_m}\right] + \left[\frac{R}{\rho_r}\right]} \tag{4}$$

M equals (Wm/WC), which is the weight percent of the matrix, and R equals (Wr/WC), which is the weight percent of reinforcement. Equation (4) can be used to estimate the true density of the composite using the weight percent of the matrix and the reinforcement as well as, their theoretical densities. In the case of HA-PEEK nanocomposites, the theoretical density of HA is 3.219 g/cm$^3$, and for PEEK, it is equal to 1.28 g/cm$^3$.

*Biological response test*

*SBF immersion test*

The ion concentrations of SBF ($SO^4$ 20.5 mM, $HPO_4$ 21.0 mM, $HCO_3$ 4.2 mM, Cl 147.8 mM, $Ca^{2+}$ 2.5 mM, $Mg^{2+}$ 1.5 mM, $K^+$ 5.0 mM, $Na^+$ 142.0 mM, pH 7.40 at 36.5 °C) are almost identical to those of human blood plasma. Kokubo's protocol was used in the preparation of the SBF solution [31]. The optimal sample of 10-weight percent Nano HA-PEEK was submerged in 40 mL of SBF at 37 °C

in a humid environment. The sample was rinsed with distilled water three times and dried at 37 °C overnight, after 14 days from immersion. SEM and energy dispersive spectrometry were used to observe and analyze the samples.

*Cell culture*

The biological response of the optimum HA-PEEK sample was examined using MC3T3-E1 cells. Before cell seeding, the samples were subject to UV sterilization for 30 min, and immersed in 70% ethanol for 1 h, then rinsed with PBS for around 15 min at least three times. MC3T3-E1 cell line was provided by the stem cell bank Pasteur Institute (Tehran, Iran). In a humidified incubator with 5% $CO^2$ in the air, at 37°C, cells were grown and maintained in Dulbecco's Modified Eagle Medium supplied with 1% PSF (antibiotic antimycotic solution) and 10% fetal bovine serum.

*Cell seeding*

After achieving around 75% confluency, Cells were detached using 0.1% ethylenediaminetetraacetic acid and 0.25% trypsin in phosphate-buffered saline (PBS) at 37°C. Then, cells were resuspended in DMEM containing 10% FBS and 1% PSF. At 10,000 cells per 24-well culture plate, five 40 µl drops of the cell suspension were gently applied to the sample's surface. The medium was introduced to cell/sample constructs after attachment had been permitted for 30 minutes.

*MTT assay*

Pre-osteoblast MC3T3-E1 proliferation on the samples was quantified using the MTT assay. MC3T3-E1 cell viability on the samples at 1,3and 5 day was estimated by using the 3-(4,5-dimethylthiazol-2-yl)-2,5 diphenyltetrazolium bromide (MTT) assay (Sigma-Aldrich, St. Louis, MO, USA).Briefly, 1 ml of 0.5 mg/ml MTT solution was added to each well, and incubated for about 4 h, then MTT solution was discarded and blue formazan was dissolved in dimethyl sulfoxide (DMSO, Merck, Germany). The absorbance was measured at 545 nm using an ELISA Reader (Stat Fax-2100, Miami, FL, USA). The cell viability was quantified using dividing the absorbance of the sample by the absorbance of control at day 1,3and 5. Date was obtained from three samples from three independent experiments (n=3).

*Fluorescent staining and microscopy analysis*

Fluorescence microscopy was also used to assess cell adherence subjectively (2.4 104 cells/well). The samples were removed from the culture media after 4 hours of cell culture, washed twice with sterile PBS, and then fixed with 4% polyoxymethylene solution. After being maintained in the dark for 20 minutes, the samples were stained with 6-diamidino-2-phenylindole dihydrochloride hydrate (DAPI, Sigma) and viewed using a DMi 6000 B fluorescence microscope (Leica, Wetzlar, Germany).

*Antibacterial test*

The antibacterial effects of HA and HA-PEEK were tested against Staphylococcus aureus (gram-positive bacteria). The S. aureus slant strains were bought from Tehran University's Laboratory of Microbiology and Biotechnology to use in the experiment. Preparing a fresh culture of the target bacteria (indicator); then Preparing a suspension of bacteria with a concentration of 0.5 McFarland (equivalent to 1.5 x 108 ml/CFU) with diluting solution (physiological serum or phosphate buffer). Depending on the sample's surface area and volume, the bacterial suspension is diluted to the appropriate cell count in the dilution solution before being applied to the sample in a specific volume (1 cc< V <0.4 cc), according to the required

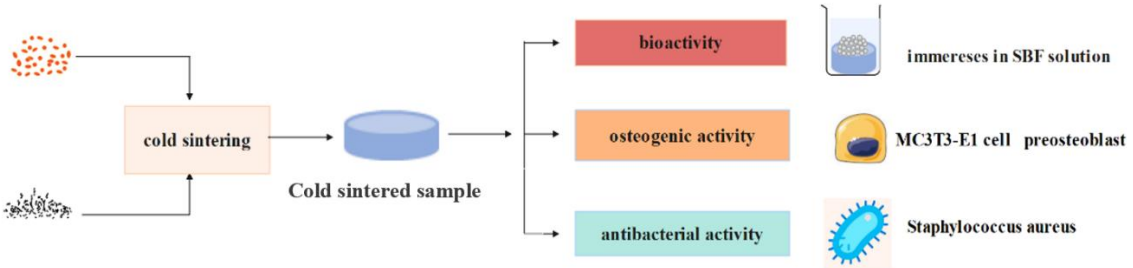


Fig. 3. Schematic diagram of Nano HA-PEEK composite biological test.

scheduling, sampling, and culture of bacteria that come in contact with the sample. A solid culture medium is spread on the surface of the plate with 0.1 cc of the sample obtained using the Plate Spread technique, and the plate is then put in an incubator set at 30 ℃. The Count Colony device will count the generated colonies after 24–48 hours. The following formula has been used for calculating the number of colonies per volume unit (ml/CFU):

CFU/ml = (no. of colonies x dilution factor) / volume of the culture plate

The lethality percentage and the logarithm of reduction are calculated based on the number of colonies per volume unit.

## RESULTS AND DISCUSSION

*Statistical Analysis*

In this study, an $L_{16}(4^4)$ Taguchi orthogonal design was used. Relative density (%), hardness (HV) and indirect tensile strength (Mpa) were taken as the performance statistics.

HA-PEEK composites produced by cold sintering, the SNL equation was utilized to identify the parameter values that maximize the density (%), hardness (HB10), and indirect tensile strength (MPa) values. The results produced by calculating the SNort statistic values for parameter levels with these SN values are illustrated in Fig. 4. a, b, and c for density, hardness, and indirect tensile strength, respectively. The SN ratio was used to generate plots by using MINITAB 21.

The relative densities of all samples range between 79% to 99%, indicating that the cold sintering process can produce the highly dense nano HA-PEEK composites. As shown in Fig. 4, the densities of the ceramic–polymer composites decrease with increasing amounts of polymer. Because the density of PEEK polymer is lighter (1.281 g/cm$^3$) than HA ceramic (3.21 g/cm$^3$).

The optimum conditions values that maximize the relative density would be a sintering temperature of 300 °C, sintering pressure of 250 bar, holding time of 60 min, and PEEK content of

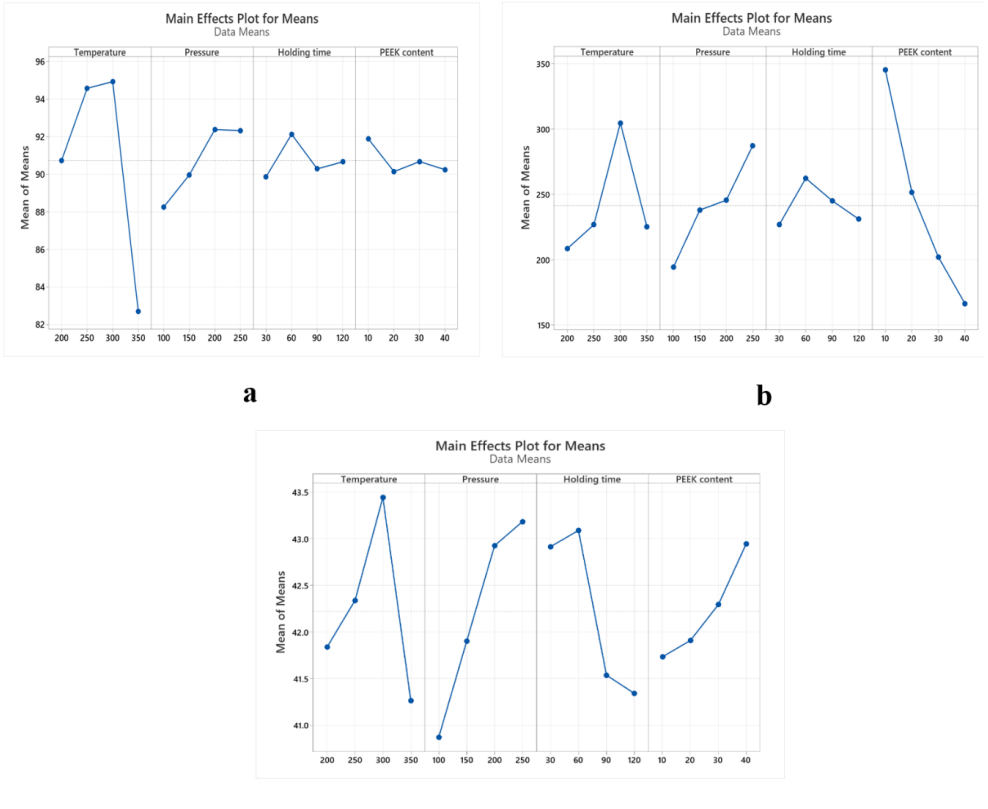


Fig. 4. $SN_{ort}$ values according to parameter levels for (a) density, (b) hardness and (c) indirect tensile strength.

10 %. Confirmation experiments were carried out twice under the same working conditions to test the predicted results. Under optimum conditions, the relative density% was predicted to be 99, which was also discovered experimentally to be 99.4%. The present case shows that the experimental and predicted values have a fair level of agreement.

Ranks were assigned based on delta values, with Rank 1 given to the highest delta value, Rank 2 to the second-highest delta value, and so on. The parameter with the greatest difference in delta value among all design parameters has the most significant effect on the response. The PEEK content had the highest delta value for the maximum value. Thus, it is the most significant parameter affecting the cold sintering process (Rank 1), while the holding time has the least effect (Rank 4). Additionally, the parameter with the largest slope has the most significant effect, whereas the parameter with the smallest slope has the least significant effect.

Time and temperature are significant factors in the dissolution of soluble substances. As a result, both time and temperature are required to move the particles into the pores. As shown in Fig. 4a, the relative density rises from 91 to 99% when the temperature rises from 200 °Cto 300 °C, then exhibits a clear reduction at 350 °C that could be caused by the water evaporating quickly at a higher cold sintering temperature, resulting in incomplete dissolution-precipitation process. When the time passed from 30 to 60 minutes, the density of the composite increased, and after that, it exhibited a minor drop. Particle rearrangement occurs via the liquid medium during the initial stage of cold sintering. The second stage involves dissolving particles under temperature and pressure, which leads to the formation of a supersaturated phase. The nucleation and densification of the composite then follow this phase. Therefore, the optimum

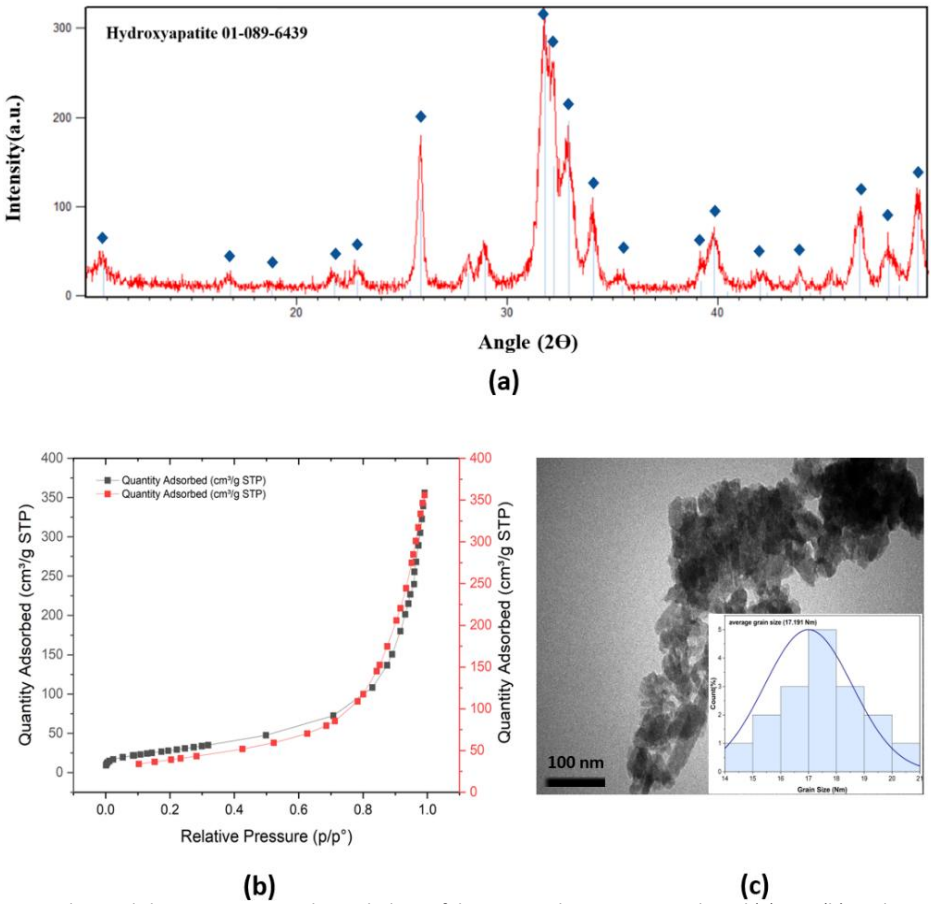


Fig. 5. Chemical characterization and morphology of the prepared nano-HA crystals: xrd (a), BET (b), and TEM image with particle size distribution (C).

temperature and time are essential for successful cold sintering densification of composites.

The parameter values maximizing the hardness would be a sintering temperature of 300 °C, a sintering pressure of 250 bar, a holding time of 60 min, and a PEEK content of 10%, as shown in Fig. 4b. Under optimum conditions, the hardness percentage was 502 HV, which is in the range of cortical bone hardness.

The parameter values maximizing the indirect tensile strength would be a sintering temperature of 300 °C, a sintering pressure of 250 bar, a holding time of 60 min, and a PEEK content of 40%, as shown in Fig. 4c. Under optimum conditions, the indirect tensile strength was 45 MPa. The elastic modulus recorded under these conditions was 5 GPa, which is in the cortical bone elastic modulus range. As PEEK content increases, the tensile strength of composites increases because the tensile strength of polymers is higher than that of ceramic.

*Characterization of nano-HA crystals*

XRD patterns of the produced HA nanopowders revealed the production of apatite as a single phase with no additional impurity phases, as shown in Fig. 5a. Each pattern matches ICDD Card 01-089-6439. Using the Scherrer formula and the full width at half maximum (FWHM) peak corresponding to the (002) plane, which is independent and does not interfere with other peaks, the average crystallite size was determined to be 17.9 nm.

TEM observed the morphologies of the obtained HA nanocrystals. Fig. 5b showed an aggregate of nanoparticles with different c/a ratios, all having a size of less than 100nm. The average crystallite sizes were 17 nm, calculated using the Image J program. Pure HA nanoparticles strongly tended to form agglomerates due to their high surface area and surface energy. This observation matches the estimated crystallite size obtained from XRD Fig. 5a.

Fig. 5c shows the plots of the adsorption and desorption isotherms of the prepared HA sample. The profile of these plots matches type II' of the six principal classes of isotherm shapes that describe the adsorption of non-porous solids [32]. The surface area values are 107, and the estimated particle size (18nm) is in full agreement with the TEM and XRD observations.

*Composition and morphology of nano HA-PEEK composite*

Fig. 6 reveals the XRD patterns of the cold-sintered nanoHA-PEEK composite samples. The sharp peaks belong to carbonated apatite, whereas the weak peaks are typical of PEEK polymer. The nano-HA particles partially encapsulating the PEEK surface reduced the intensity of the PEEK main peaks in the nano-HA-PEEK composite. The formation of B-type carbon-substituted apatite is caused by the ion exchange in the crystal structure of HA during the composite preparation process. It is similar to the apatite located in the bone [33].

SEM images with EDS mapping of the optimum cold sintered composite sample are shown in

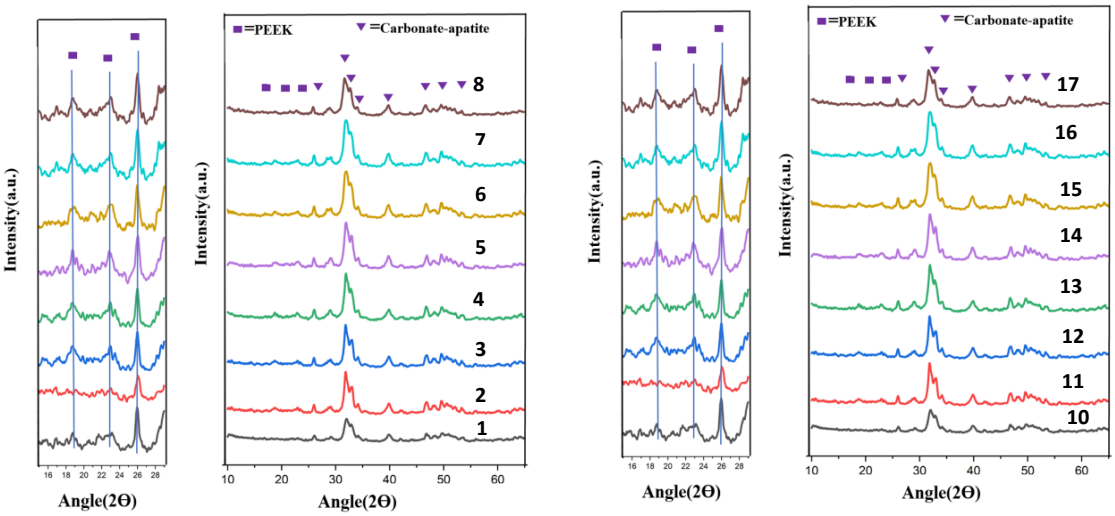


Fig. 6. XRD graphics of 16 nano HA-PEEK composite.

Figs. 7a–d. Two separate phases are found in the sample, revealing dense microstructures that conform to the XRD results (Fig. 6). Along with the HA grains, PEEK particles can be uniformly distributed, and in some areas, the HA can cover the PEEK grains. This agreement is with the energy dispersive X-ray spectrum (EDS) analysis (Fig. 7c), where the green and purple contrast regions belong to PEEK and HA phases, respectively. Fig. 8 shows the particle size distribution, where the

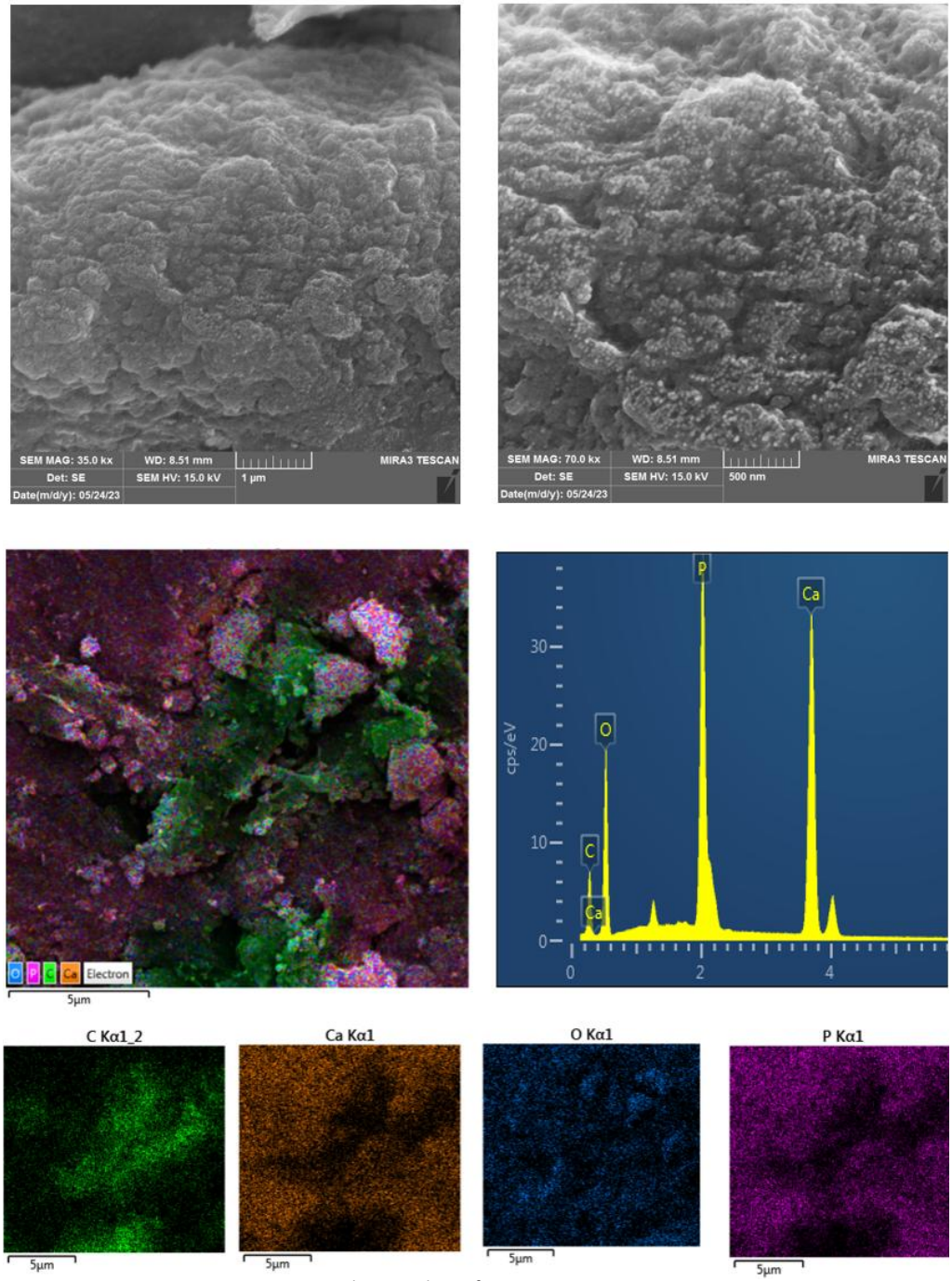


Fig. 7. SEM and EDS analysis of 16 nano HA-PEEK composite.

average particle size of the optimum sample is (40 nm). The increment in particle size is attributed to the densification process during sintering.

*Contact angle result*

The water contact angle is a convenient way to assess the wettability and biocompatibility of composite surfaces. The contact angles of pure HA and the optimal sample of composite are 28° and 33°, respectively. According to Fig. 9, it can be noticed that all samples exhibit good hydrophilic properties because of their hydrophilicity, which is attributed to the existence of -OH groups on their surface. The nano HA-PEEK composite does not affect the hydrophobicity of PEEK, and it remains hydrophilic due to the HA particles partially covering the PEEK surface. In order to attain great surface coverage (hydrophilic), a low contact angle is often preferable. It has been demonstrated that the maximum degrees of cell attachment, protein adsorption, platelet adhesion/activation, and blood coagulation are stimulated by hydrophilic

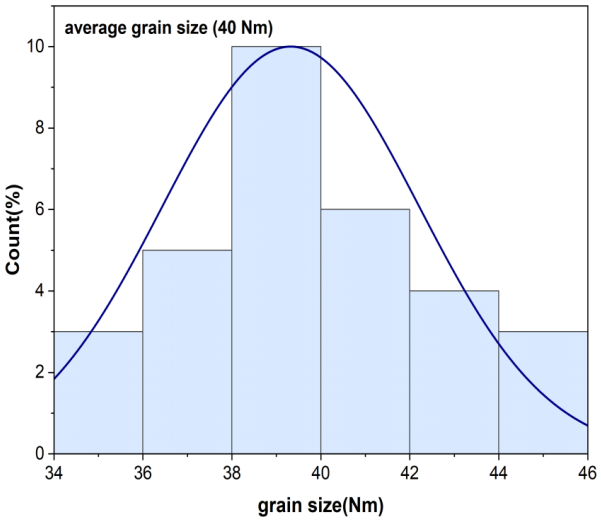


Fig. 8. particle size distribution of HA-PEEK composite.

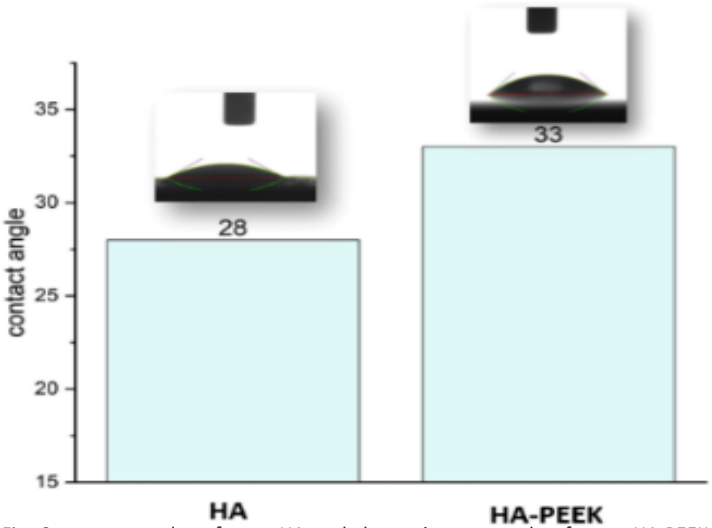


Fig. 9. contact angles of pure HA and the optimum sample of nano HA-PEEK composite.

surfaces.

*Biological response*

*Bone-like apatite formation*

The optimum sample of nano HA-PEEK composite was immersed in a simulated body to investigate its bioactivity. Fig. 10 shows the SEM images and EDS spectra results of the nano HA-PEEK composite after immersion in SBF for 14 days. These indicated that the Nano HA-PEEK composite is a good bioactive material. The bioactive material interacts with the surrounding bone more successfully due to its ability to promote apatite formation[10].

*Initial cell adhesion*

The adhesion is one of the earliest biological responses of cells to biomaterials. By observing the behavior of the cells, it was possible to monitor how the addition of PEEK affected the biocompatibility of HA. After 1,3,5 day of cell culture, the adhesion effectiveness of pre-osteoblasts on pure HA and

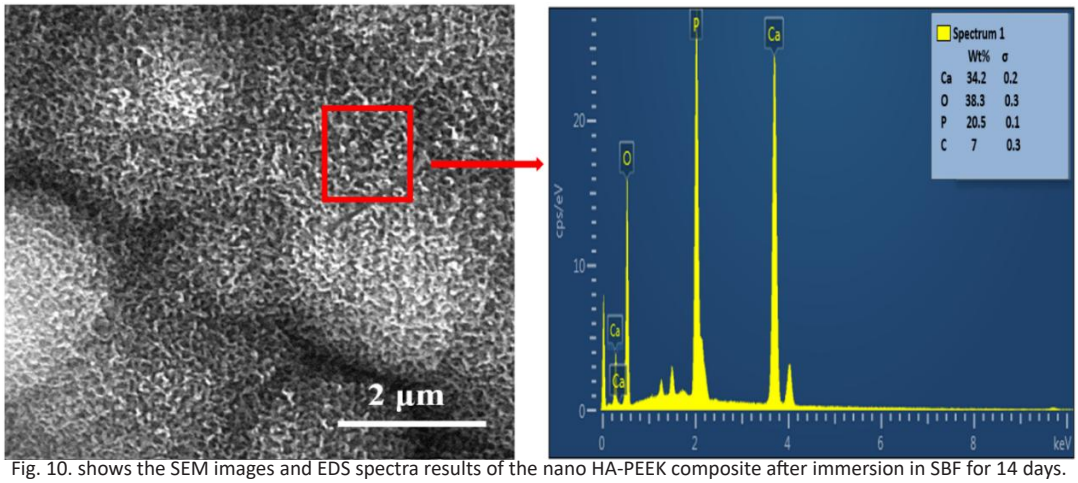


Fig. 10. shows the SEM images and EDS spectra results of the nano HA-PEEK composite after immersion in SBF for 14 days.

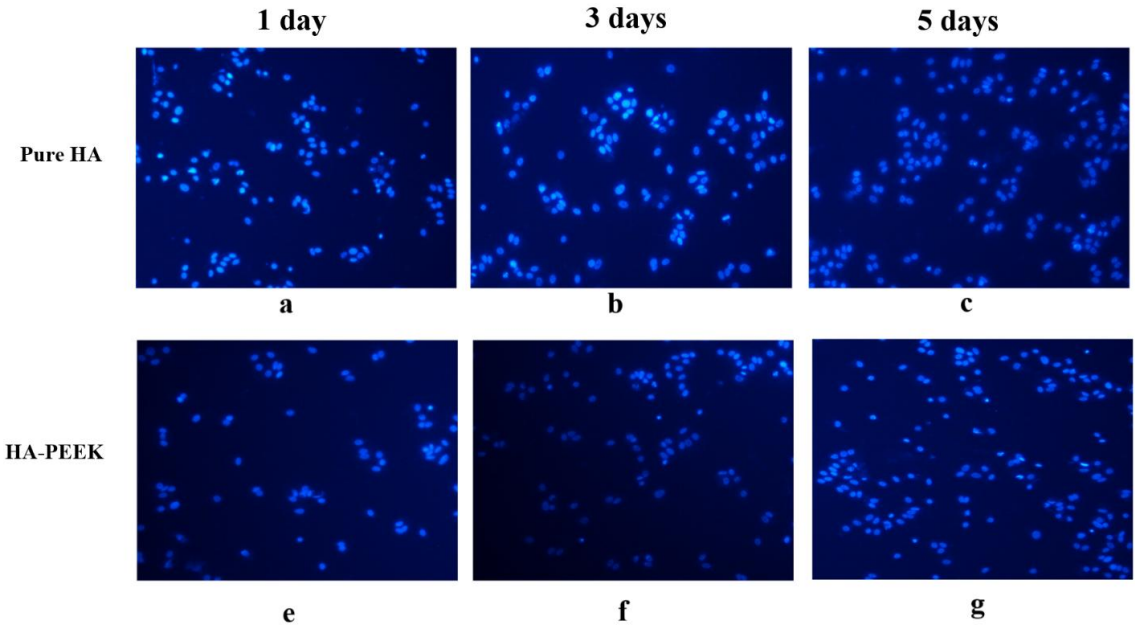


Fig. 11. Fluorescence micrographs of MC3T3-E1 pre-osteoblast (nuclei in blue) adhesion measured on pure HA (a-c) and optimum HA-PEEK composite after incubation for 1,3 and 5 days.

optimum nano HA-PEEK composite was assessed. At 1 and 3 days, more cells were observed on the HA surface compared to the HA-PEEK composite, as shown in Fig. 11(a-g) and Fig. 12. There was no significant difference in the number of living cells observed in the two material groups on the fifth day, indicating better cell attachment. It agrees with contact angle results showing that HA is hydrophilic due to its hydroxyl groups on its surface, resulting in the ability of HA to attract osteoblasts. It stimulates cell proliferation and osteogenic differentiation of osteoblast cells [3].

*Cell proliferation*

Pre-osteoblast proliferation on the samples was assessed using an MTT viability test, as shown in Fig. 12. After 1 day of incubation, it is obvious that cell proliferation on HA is somewhat

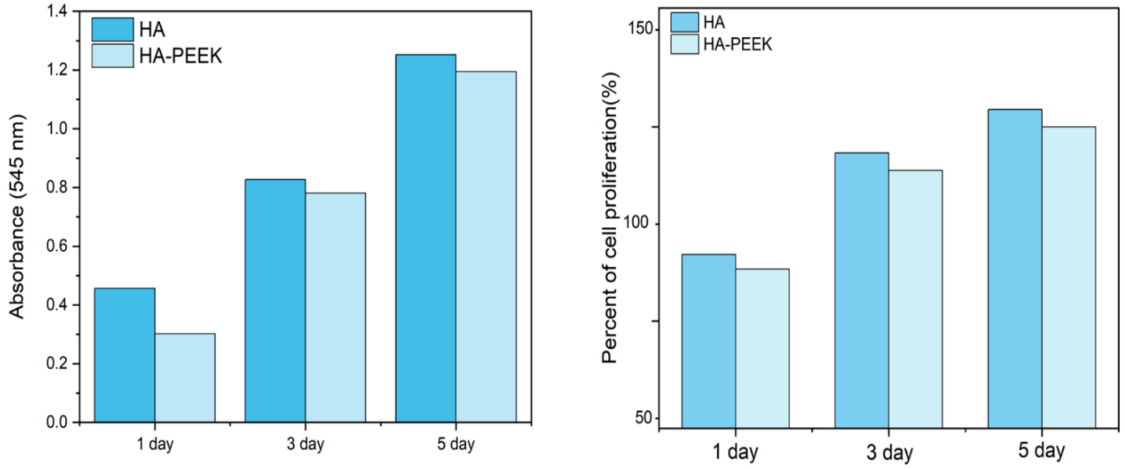


Fig. 12. Cell adhesion (A) and cell proliferation (B) of MC3T3-E1 pre-osteoblasts cultured on pure HA and HA-PEEK composite for 1, 3, and 5 days.

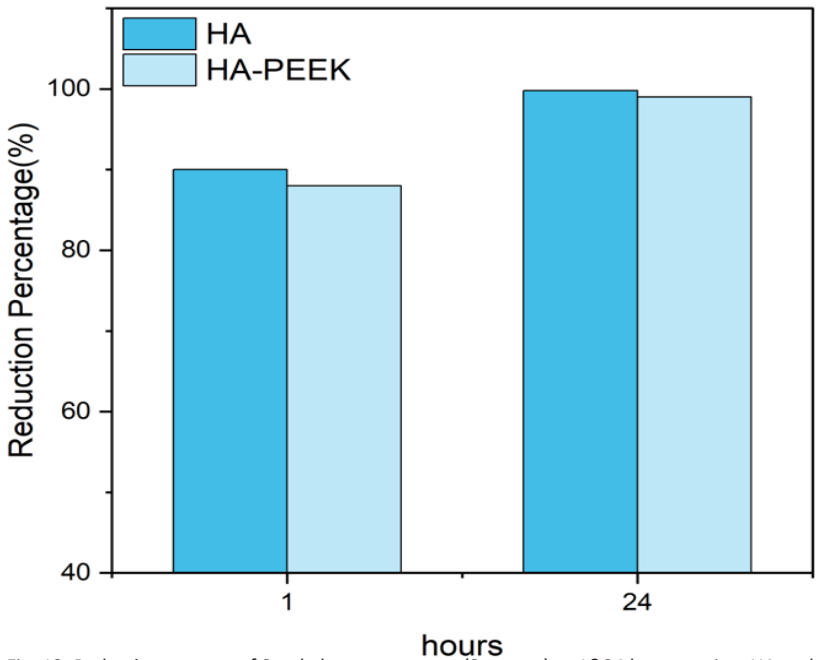


Fig. 13. Reduction percent of Staphylococcus aureus (S.aureus) at 1&24 hours against HA and HA-PEEK composite.

higher than that on HA-PEEK. However, at 3 and 5 days, the cells on HA-PEEK composite surfaces appear to have greater rates of proliferation and viability, indicating that HA-PEEK composite has beneficial effects on the proliferation of cells. These results conform to the contact angle results that show the surface of HA-PEEK has hydrophilic properties, which improve osteoblast spreading and proliferation. It has been shown that hydrophilic surfaces are more preferable than hydrophobic surfaces for cell adhesion, proliferation, and differentiation to enhance bone repair. It is commonly recognized that the early contacts between the cells and implant surface are essential for clinical success and that advancement may accelerate bone formation [34]. Overall, the results of this study illustrate that cell adhesion, spreading, and proliferation are gradually increasing with time in both samples, and no cytotoxic effects can be found on the MC3T3-E1 cells.

*Antibacterial results*

In the method of counting the number of living

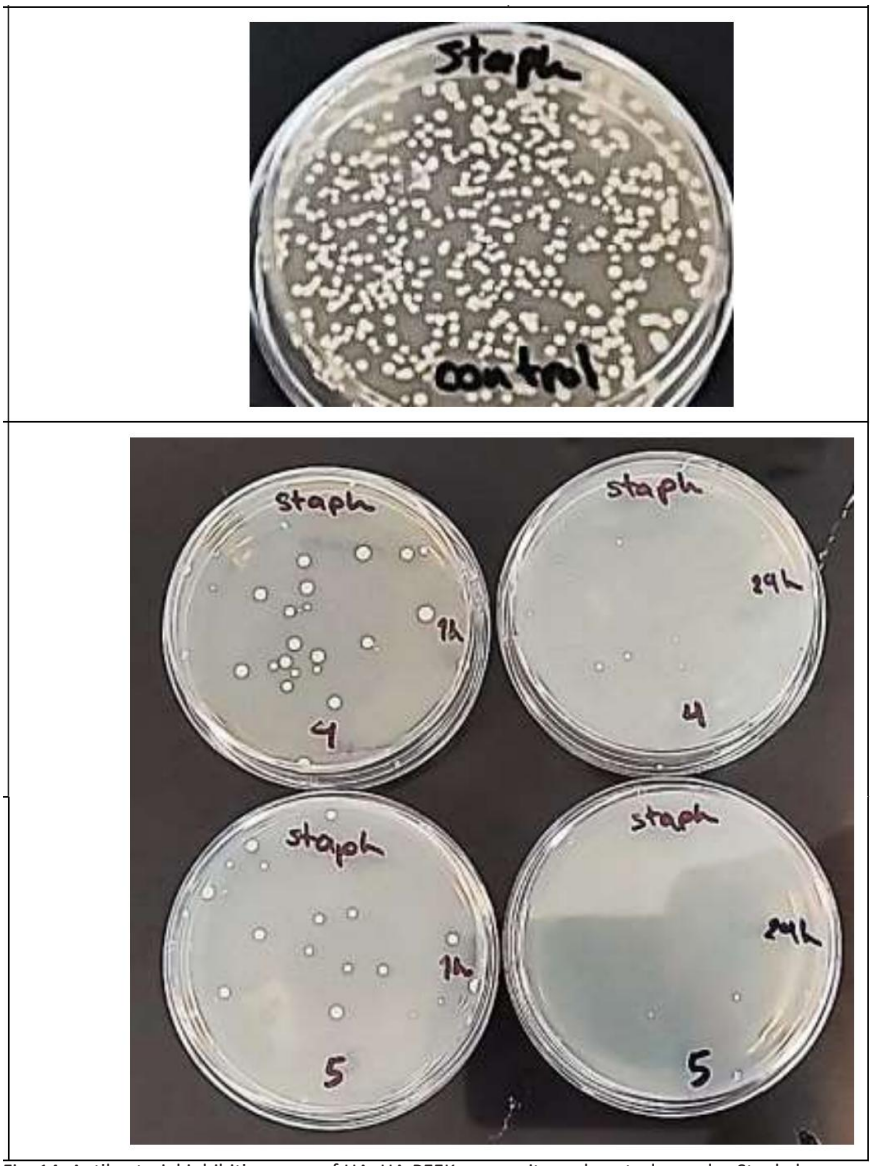


Fig. 14. Antibacterial inhibition zone of HA, HA-PEEK composite and control samples Staphylococcus aureus (S.aureus) at 1 and 24 hours.

cells, due to the fact that the contact between bacteria and matter is established dynamically, the antibacterial property of the samples can be checked more and faster. Both substances were reported to have an antibacterial effect of 95% in one hour and more than 99.9% in 24 hours. In this method, no special difference was observed between samples HA and HA-PEEK (Figs. 13 and 14).

## CONCLUSION

In the present work, the Cold sintering process shows the ability to produce composite material with high-volume fractions of ceramic. The Taguchi robust design $L_{16}$ orthogonal array was used to evaluate the optimum cold sintering parameters. The main conclusions can be drawn:

1. The optimum conditions values that maximize the relative density would be a sintering temperature of 300 °C, sintering pressure of 250 bar, holding time of 60 min, and PEEK content of 10 %. Under optimum conditions, the relative density% was predicted to be 99, which was also discovered experimentally to be 99.4%. The present case shows that the experimental and predicted values have a fair level of agreement.
2. Under optimum conditions, the hardness percentage was 502 HV, which is in the range of cortical bone hardness.
3. The parameter values maximizing the indirect tensile strength would be a sintering temperature of 300 °C, a sintering pressure of 250 bar, a holding time of 60 min, and a PEEK content of 40%. Under optimum conditions, the indirect tensile strength was 45 MPa.
4. According to contact angle results, all samples exhibit good hydrophilic properties.
5. After 14 days of immersion in SBF, apatite islands developed on the HA-PEEK composite, indicating excellent bioactivity.
6. In vitro test, the HA-PEEK composite exhibited good pre-osteoblast cell (MC3T3-E1) adhesion, spreading, and proliferation. In this study, the cold sintering process used to produce composite material with mechanical and biological properties close to bone makes it a good candidate for applying orthopedic and dental implants.

## CONFLICT OF INTEREST

The authors declare that there is no conflict of interests regarding the publication of this manuscript.

## REFERENCES


1. Ma R, Tang T. Current Strategies to Improve the Bioactivity of PEEK. Int J Mol Sci. 2014;15(4):5426-5445.
2. Briem D, Strametz S, Schröoder K, Meenen NM, Lehmann W, Linhart W, et al. Response of primary fibroblasts and osteoblasts to plasma treated polyetheretherketone (PEEK) surfaces. J Mater Sci Mater Med. 2005;16(7):671-677.
3. Ma R, Guo D. Evaluating the bioactivity of a hydroxyapatite-incorporated polyetheretherketone biocomposite. J Orthop Surg Res. 2019;14(1).
4. Akram W, Zahid R, Usama RM, AlQahtani SA, Dahshan M, Basit MA, et al. Enhancement of Antibacterial Properties, Surface Morphology and In Vitro Bioactivity of Hydroxyapatite-Zinc Oxide Nanocomposite Coating by Electrophoretic Deposition Technique. Bioengineering. 2023;10(6):693.
5. Kokubo T, Kim H-M, Kawashita M. Novel bioactive materials with different mechanical properties. Biomaterials. 2003;24(13):2161-2175.
6. Ma R, Weng L, Bao X, Ni Z, Song S, Cai W. Characterization of in situ synthesized hydroxyapatite/polyetheretherketone composite materials. Mater Lett. 2012;71:117-119.
7. Abu Bakar MS, Cheng MHW, Tang SM, Yu SC, Liao K, Tan CT, et al. Tensile properties, tension–tension fatigue and biological response of polyetheretherketone–hydroxyapatite composites for load-bearing orthopedic implants. Biomaterials. 2003;24(13):2245-2250.
8. Tang S. Tension–tension fatigue behavior of hydroxyapatite reinforced polyetheretherketone composites. Int J Fatigue. 2004;26(1):49-57.
9. Wong KL, Wong CT, Liu WC, Pan HB, Fong MK, Lam WM, et al. Mechanical properties and in vitro response of strontium-containing hydroxyapatite/polyetheretherketone composites. Biomaterials. 2009;30(23-24):3810-3817.
10. Tang T, Ma R, Tang S, Tan H, Lin W, Wang Y, et al. Preparation, characterization, and in vitro osteoblast functions of a nano-hydroxyapatite/polyetheretherketone biocomposite as orthopedic implant material. International Journal of Nanomedicine. 2014:3949.
11. Converse GL, Yue W, Roeder RK. Processing and tensile properties of hydroxyapatite-whisker-reinforced polyetheretherketone. Biomaterials. 2007;28(6):927-935.
12. Converse GL, Conrad TL, Roeder RK. Mechanical properties of hydroxyapatite whisker reinforced polyetherketoneketone composite scaffolds. J Mech Behav Biomed Mater. 2009;2(6):627-635.
13. Converse GL, Conrad TL, Merrill CH, Roeder RK. Hydroxyapatite whisker-reinforced polyetherketoneketone bone ingrowth scaffolds. Acta Biomater. 2010;6(3):856-863.
14. Yu S, Hariram KP, Kumar R, Cheang P, Aik KK. In vitro apatite formation and its growth kinetics on hydroxyapatite/polyetheretherketone biocomposites. Biomaterials. 2005;26(15):2343-2352.
15. Hengky C, Kelsen B, Saraswati, Cheang P. Mechanical and Biological Characterization of Pressureless Sintered Hydroxapatite-Polyetheretherketone Biocomposite. IFMBE Proceedings: Springer Berlin Heidelberg; 2009. p. 261-264. http://dx.doi.org/10.1007/978-3-540-92841-6_63
16. Tan KH, Chua CK, Leong KF, Cheah CM, Cheang P, Abu Bakar MS, et al. Scaffold development using selective laser sintering of polyetheretherketone–hydroxyapatite biocomposite blends. Biomaterials. 2003;24(18):3115-3123.

17. Schmidt M, Pohle D, Rechtenwald T. Selective Laser Sintering of PEEK. CIRP Annals. 2007;56(1):205-208.
18. Tan KH, Chua CK, Leong KF, Naing MW, Cheah CM. Fabrication and characterization of three-dimensional poly(ether-ether-ketone)/-hydroxyapatite biocomposite scaffolds using laser sintering. Proceedings of the Institution of Mechanical Engineers, Part H: Journal of Engineering in Medicine. 2005;219(3):183-194.
19. Si M, Hao J, Zhao E, Zhao X, Guo J, Wang H, et al. Preparation of zinc oxide/poly-ether-ether-ketone (PEEK) composites via the cold sintering process. Acta Mater. 2021;215:117036.
20. Maria J-P, Kang X, Floyd RD, Dickey EC, Guo H, Guo J, et al. Cold sintering: Current status and prospects. J Mater Res. 2017;32(17):3205-3218.
21. Hérisson de Beauvoir T, Tsuji K, Zhao X, Guo J, Randall C. Cold sintering of ZnO-PTFE: Utilizing polymer phase to promote ceramic anisotropic grain growth. Acta Mater. 2020;186:511-516.
22. Funahashi S, Guo J, Guo H, Wang K, Baker AL, Shiratsuyu K, et al. Demonstration of the cold sintering process study for the densification and grain growth of ZnO ceramics. J Am Ceram Soc. 2016;100(2):546-553.
23. de Beauvoir TH, Dursun S, Gao L, Randall C. New Opportunities in Metallization Integration in Cofired Electroceramic Multilayers by the Cold Sintering Process. ACS Applied Electronic Materials. 2019;1(7):1198-1207.
24. Wang D, Zhou D, Zhang S, Vardaxoglou Y, Whittow WG, Cadman D, et al. Cold-Sintered Temperature Stable $Na_{0.5}Bi_{0.5}MoO_4$–$Li_2MoO_4$ Microwave Composite Ceramics. ACS Sustainable Chemistry and Engineering. 2018;6(2):2438-2444.
25. Ndayishimiye A, Grady ZA, Tsuji K, Wang K, Bang SH, Randall CA. Thermosetting polymers in cold sintering: The fabrication of ZnO-polydimethylsiloxane composites. J Am Ceram Soc. 2020;103(5):3039-3050.
26. Coutinho L, Aredes RG, Antonelli E. Cold sintering and electric characterization of ZnO-BaTiO3 composites. Cerâmica. 2021;67(381):105-110.
27. Induja IJ, Sebastian MT. Microwave dielectric properties of cold sintered $Al_2O_3$-NaCl composite. Mater Lett. 2018;211:55-57.
28. KüÇük ö. Application of Taguchi method in the optimization of dissolution of ulexite in NH4Cl Solutions. Korean J Chem Eng. 2006;23(1):21-27.
29. Küçük Ö, Elfarah T, Islak S, Özorak C. Optimization by Using Taguchi Method of the Production of Magnesium-Matrix Carbide Reinforced Composites by Powder Metallurgy Method. Metals. 2017;7(9):352.
30. Daniels N. Am I My Parents' Keeper? Midwest Studies in Philosophy. 1982;7:517-540.
31. Kokubo T, Takadama H. How useful is SBF in predicting in vivo bone bioactivity? Biomaterials. 2006;27(15):2907-2915.
32. Haul R. S. J. Gregg, K. S. W. Sing: Adsorption, Surface Area and Porosity. 2. Auflage, Academic Press, London 1982. 303 Seiten, Preis: $ 49.50. Berichte der Bunsengesellschaft für physikalische Chemie. 1982;86(10):957-957.
33. Deng Y, Sun Y, Chen X, Zhu P, Wei S. Biomimetic synthesis and biocompatibility evaluation of carbonated apatites template-mediated by heparin. Materials Science and Engineering: C. 2013;33(5):2905-2913.
34. Zheng Y, Xiong C, Zhang S, Li X, Zhang L. Bone-like apatite coating on functionalized poly(etheretherketone) surface via tailored silanization layers technique. Materials Science and Engineering: C. 2015;55:512-523.